ELSEVIER

MXene guides microwaves through 3D polymeric structures

Omid Niksan [a], Lingyi Bi [b,c], Kasra Khorsand Kazemi [a], Roman Rakhmanov [c,d], Yury Gogotsi [b,c,*], Mohammad H. Zarifi [a,*]

[a] Faculty of Applied Sciences, School of Engineering, University of British Columbia, Kelowna, BC V1V1V7, Canada
[b] Department of Materials Science and Engineering, Drexel University, Philadelphia, PA 19104, USA
[c] A.J. Drexel Nanomaterials Institute, Drexel University, Philadelphia, PA 19104, USA
[d] Department of Electrical and Computer Engineering, Drexel University, Philadelphia, Pennsylvania 19104, USA

With the advances in space technology, weight reduction of components has been a paramount, yet challenging task. Additive manufacturing with high-performance polymers can realize lightweight and complex geometries that can also be manufactured on board. Yet polymers are electromagnetically inefficient for applications requiring electrical conductivity, such as guiding microwave signals. This work presents high-efficiency and lightweight additively-manufactured microwave components enabled by MXene coating. The waveguiding functionality was observed from 8 to 33 GHz, covering low earth orbit (LEO) frequencies, with a power-handling capability of up to 10 dB and a transmission coefficient of 93 %. After a single dip-coating cycle, the polymer waveguide performed only 2 % below an eight times heavier metallic equivalent. Frequency/polarization filtering was enabled by implementing special geometries, and a range of microwave functionalities, including resonance, was demonstrated. The MXene-coated components can replace 3D-printed and bulk metals, greatly decreasing weight and cost in space, and also in various terrestrial applications.

Keywords: MXene; Microwaves; Waveguide Components; Additive Manufacturing; Lightweight

Introduction

The impact of additive manufacturing has been significantly increasing in the advancing technological domains, such as aerospace technology, where unique and application-dependent geometries are employed in aerial vehicles and satellites [1]. Quick production of a limited number of components for low-volume manufacturing and rapid prototyping is critical. Metal additive manufacturing (AM) offers the potential to fabricate hollow components that are relatively lightweight, with complex geometries increasingly demanded by new aerial vehicles and satellite designs that are outside the reach of traditional metallurgy [2]. Still, the mass density of metals, along with the cost and complexity of laser sintering, limits the utility of metal AM, especially in space. The usage of polymeric components through AM processes, on the other hand, has great cost and weight-related benefits [3]. However, polymeric materials often do not meet certain property requirements, such as high electrical conductivity [4], that are integral to the functionality of modern communication systems [5].

With satellite technology marking new advancements through the commercialization of Low Earth Orbit (LEO) launches, communication devices are increasingly demanded to allow for low-latency telecommunication capability and extensive coverage [6]. To date, five primary constellations (companies) have launched ~ 15000 LEO satellites that utilize microwave frequencies (in particular, Ku-Ka bands) in the

* Corresponding authors.
E-mail addresses: Gogotsi, Y. (gogotsi@drexel.edu), Zarifi, M.H. (mohammad.zarifi@ubc.ca).

 https://doi.org/10.1016/j.mattod.2023.12.013

communication devices [7]. To guarantee low loss of microwave signals and to handle high-power transmission, bulky metallic components, such as waveguides are utilized [8–11]. To lower the mass load of fully-metal components, thin layers of metals can be deposited on polymer structures [12,13]. Application of thin metal coatings onto planar, non-conductive substrates (e.g., polymers or ceramics) enables microwave structures that introduce various functionalities, such as resonators or sensors, that be used as part of modern communication devices [14–19]. However, such techniques as electroless deposition of metals onto polymer substrates presents challenges, including but not limited to a restricted selection of metals/substrates, thermal stability of substrates and process temperature control, as well as adverse environmental effects [20,21]. Metal paints, including those containing silver flakes, nanoparticles, or nanowires, have been explored [22]. However, stabilizing metal particles—crucial for solution processing like dip coating—requires a complex mixture of stabilizers, additives, organic solvents, and binders. Since these components are nonconductive, they have a detrimental impact on electrical conductivity. Moreover, typically used solvents, such as N-methyl-2-pyrrolidone (NMP), are toxic and necessitate high-temperature removal (typically at 120–150 °C) after the paint/ink is applied to a substrate. This places constraints on the choice of polymers.

Two-dimensional (2D) transition metal carbides and nitrides, MXenes, have attracted significant attention due to their distinctive properties, particularly high electrical conductivity, solution processibility at ambient conditions, and thermal shock stability [23]. In contrast to metals (e.g., copper), the 2D morphology with functional surface terminations allows MXenes to form stable colloids in water and polar organic solvents, without the need for additives or surfactants, enabling their easy processibility [24]. MXenes have been demonstrated as an additive-free coating material that can be applied to a variety of substrates of any shape (e.g., foams, glass, textiles). They conformally cover substrate surfaces [25]. Among more than 50 compositions of MXenes synthesized, $Ti_3C_2T_x$, the first discovered and most studied, has undergone extensive synthesis optimization which resulted in an electrical conductivity of up to 24,000 S/cm, the highest among solution-processable 2D materials [26,27] and high oxidation stability [26]. MXene's remarkable electrical conductivity enables the near-ideal reflection of microwaves, a functionality that was exclusive to metals [28,29]. This property has been assessed in realizing microwave transmission lines [30], planar antennas [4,31], and thin free-standing films as microwave resonators [32,33], demonstrating comparable performance with conventional metallic implementations. Moreover, the application of MXene is remarkably straightforward, comprising only MXene and water [25]. The simple formulation produces a highly conductive coating as soon as the water is evaporated at room temperature, during which MXene's surface functional groups facilitate adhesion to the substrate. This higher electrical conductivity allows the use of thinner coatings, which are conformal and smooth. The integration of MXene with lightweight, unconventionally shaped geometries holds promise for the development of next-generation communication devices with multiple features and functions.

Here we have demonstrated, for the first time, the application of electrically conductive MXene from a water-based MXene (colloidal) solution to polymeric AM components (nylon channels) through a straightforward dip coating process. Dip coating is preferred over spray coating because it allows for the use of more concentrated (viscous) MXene solutions, can be used to coat narrow channels of complex shapes, and does not require any special equipment [34]. $Ti_3C_2T_x$ was synthesized by selective chemical etching of the Al atoms from the parent Ti_3AlC_2 MAX phase using a previously reported mixed acids method [35]. The formation of single-flake MXene dispersions was confirmed by transmission electron microscopy (Fig. 1A inset), demonstrating successful etching and exfoliation. The substrate chosen for coating was commercially available nylon PA-12. This choice was informed by our prior work, where X-ray Photoelectron Spectroscopy (XPS) suggested strong bonding, potentially covalent interactions, between $Ti_3C_2T_x$ MXene and nylon, providing robust adhesion between the two materials [36–40]. A selective laser sintering (SLS) printing method was adopted with the selection of a rougher printing resolution (on the micrometer scale) for enhancing MXene coating adhesion through mechanical entrapment. Correlations were observed between the thickness of the MXene layers and microwave performance. The facile MXene coating enables a highly efficient, three-dimensional manipulation of electromagnetic waves within channels. The microwave-associated functionalities were demonstrated at different power levels and in the frequency span of 8 GHz to 33 GHz, covering the already-in-use operation range in LEO satellite communication. Various MXene dip-coated geometries, including straight, bent, twist, and resonator sections were implemented and repetitively measured using microwave equipment.

Results and discussion

Fig. 1 demonstrates the performance and weight comparison of the MXene-coated and metallic structures for a straight waveguiding section operating at the Ku band (12.4–18 GHz). In Fig. 1A, the weights of a nylon waveguide before coating, the same waveguide after one cycle of MXene coating, and a commercial waveguide made of aluminum (measurements in Fig. S2) are compared. The waveguide coated with MXene exhibited a significantly lower (8.2 times lower) weight compared to the conventional aluminum waveguide. Comparing the weights before and after coating, a single cycle of dip coating added only 0.1 g or 0.62 % of the weight of the uncoated nylon structure. Investigating electromagnetic power transmission and reflection within a straight rectangular waveguiding channel establishes a performance comparison between the MXene-coated guides and metallic waveguides. Therefore, the transmission coefficients of the MXene-coated straight waveguide were compared to a metallic one in Fig. 1B. The waveguiding performance was analyzed by measuring the transmission coefficient of electromagnetic waves, propagating from port 1 of the structure to port 2 (Fig. 1B inset and Fig. S3). The magnitude of S_{21} (dB) measurements was used as an equivalent parameter to the transmission coefficient (relation to insertion loss is reported in the

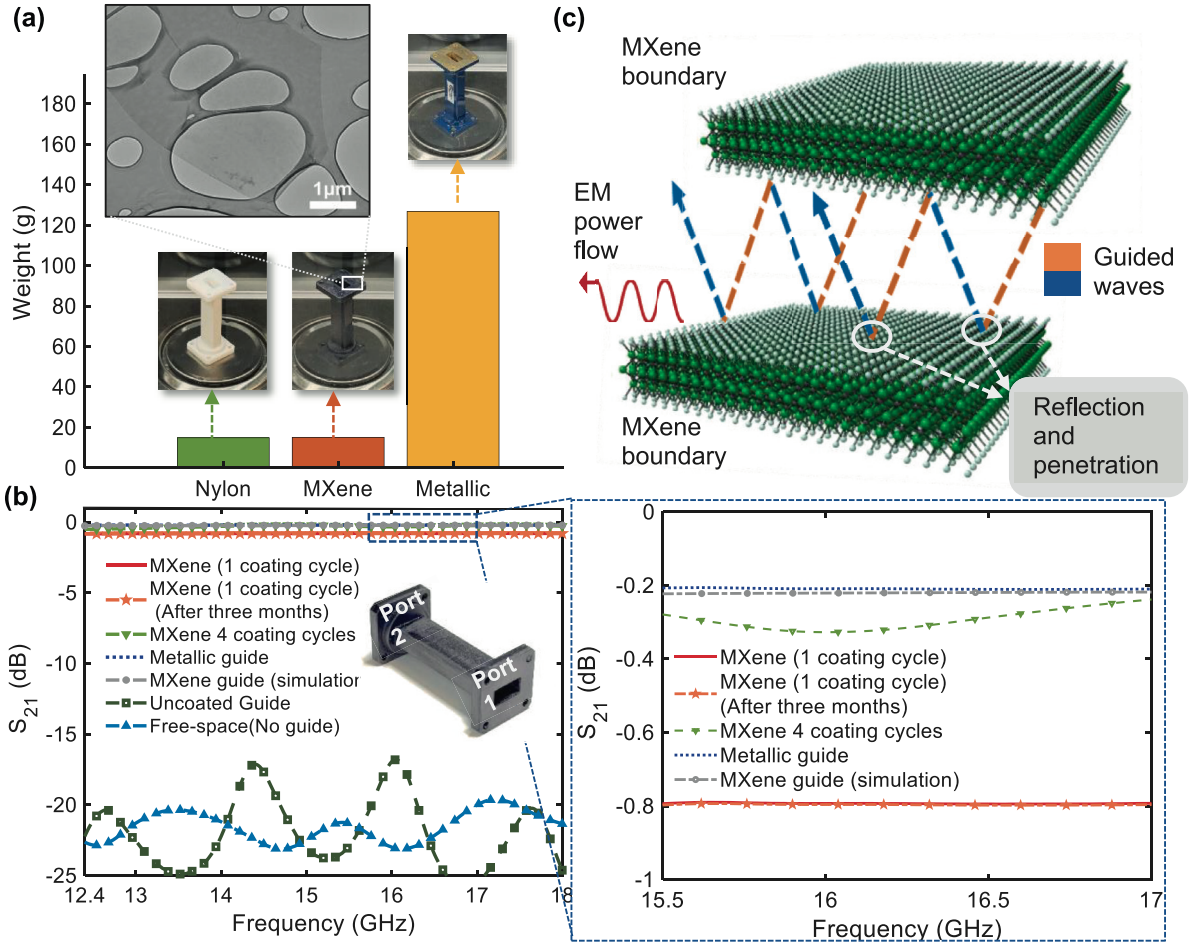

FIG. 1

Performance and weight comparison of MXene-coated straight waveguide with conventional metallic waveguides. (A) Weight comparison of an uncoated nylon structure, a MXene-coated straight waveguide, and a metallic waveguide on a digital scale. Inset shows a TEM image of a ~ 1-nm thin MXene flake. (B) The measured and simulated transmission coefficient of electromagnetic waves propagating through different mediums including MXene waveguide, metallic waveguide, 3D printed uncoated structure and free space (no waveguiding structure). (C) The illustration of waveguiding functionality using $Ti_3C_2T_x$ MXene coated walls.

Supplementary Information). MXene coated straight waveguide section showed only ~ 2.3 % decrease in the electromagnetic waveguiding performance (-0.1 dB reduction in transmission coefficient). After only one cycle of MXene coating, the experimentally measured transmission coefficient was −0.9 dB, indicating an 81 % efficiency for guiding the electromagnetic waves between two excitation terminals (Fig. 1B). The stability of the guides was experimentally investigated after three months of environmental exposure showing a negligible reduction in performance (Fig. S4).

It is understood that the guiding of electromagnetic waves is affected by each incidence of waves on the conducting MXene walls [41]. At each incidence, a portion of power will penetrate and dissipate in a conductor, leading to a loss. The remaining portion of EM power at each incident would be reflected by the conducting boundary (as illustrated by red and blue dashed lines in Fig. 1C) giving rise to the guiding mechanism [41,42]. The conductivity-dependent loss of MXene-coated structures can be described through the mechanism of wave penetration into a body with finite uniform conductivity. The power penetrated into the body of a conductor, P_{loss} is correlated with a dissipative term defined as the "surface resistance", R_s ($P_{loss} \propto R_s$) [5]:

$$R_s = \sqrt{\frac{2\pi f \mu}{2\sigma}} \quad (1)$$

where f is the frequency of an incident wave on the waveguide walls, with σ and μ representing the bulk conductivity and permeability of the bulk conductor, respectively. Eq. (1) indicates the increase in the conductivity of the conductor walls decreases the dissipative loss, R_s, minimizing the loss of energy (heat dissipation) for a wave propagating in the guide. An ideal medium (or material) exhibiting infinitely high bulk conductivity becomes lossless at microwave frequencies. This can then lead to a perfect reflection of waves from surfaces, particularly useful for guiding applications. The relations of Eq. (1) also imply a frequency-dependent loss mechanism upon wave guiding, where the waves carrying a higher frequency (f) propagate with the characteristics of higher dissipated power. The higher the ratio of reflection, the less penetration and dissipation inside the conductor body.

A parametric study was conducted to optimize the MXene coating and examine the impact of MXene size and dip coating on reflection performance (Fig. 2). The hypothesis is that MXene flake size and coating thickness influence the reflection performance. It is known that larger MXene flake sizes result in 1) higher electrical conductivity, leading to more effective reflection, and 2) increased viscosity, resulting in thicker MXene deposition. MXene dispersions with three different flake sizes (1300 nm, 500 nm, and 200 nm) were prepared at the same 20 mg/ml MXene concentration through sonication-assisted size reduction and processed into freestanding films of the same weight (20 mg) via vacuum-assisted filtration for electrical conductivity measurements (Fig. 2A and Fig. S5). The electrical conductivities of the three films decreased with flake size from approximately 13,100 S/cm to 11,500 S/cm and 5400 S/cm. Identical 3D printed coupons with representative roughness for 3D printed nylon parts were prepared, and they underwent up to five dip coating cycles in the MXene dispersions. No surface modification was performed before MXene dip coating due to the chemical compatibility between nylon and MXene. Each coupon was immersed in the designated MXene dispersion for one minute and allowed to dry completely before the next dip coating cycle (Fig. S6). It is worth noting that as the MXene size increased, longer waiting times (less preferable for production) were required for the coating to dry, ranging from 10 min to 2 h and 18 h for small, medium, and large-sized MXene flakes respectively. As anticipated, the MXene loading increased with both the MXene flake size and the number of dip coating cycles (Fig. 2B). Although all flake sizes provided complete coverage of the nylon coupons from the first dip, the effect of increasing viscosity due to flake size was evident in the smoother film-like coating morphology of the large MXene dip coated coupons, compared to the rougher and more conformal coating provided by the medium and small-sized coupons (Fig. 2B inserts and Fig. S7). To understand the effect of flake size and dip coating cycles on MXene coating, the ratio between the actual surface area and the projected area was calculated using the Developed Interfacial Area Ratio (Sdr) obtained from laser confocal scans (Fig. S8). Distinct trends were observed for MXene flakes of different sizes. While small flakes had little effect on the surface area, indicating a highly conformal coating, large flakes provided a decrease in surface area due to MXene coating forming films that leveled the rough surface. To our surprise, medium-sized MXene flakes exhibited the largest increase in surface area and changes in roughness throughout the five dip coating cycles (Fig. S9). We speculate that medium flakes had difficulty in flake packing on substrates of this particular roughness, leading to chaotic flake alignment on the surface and an increase in surface area.

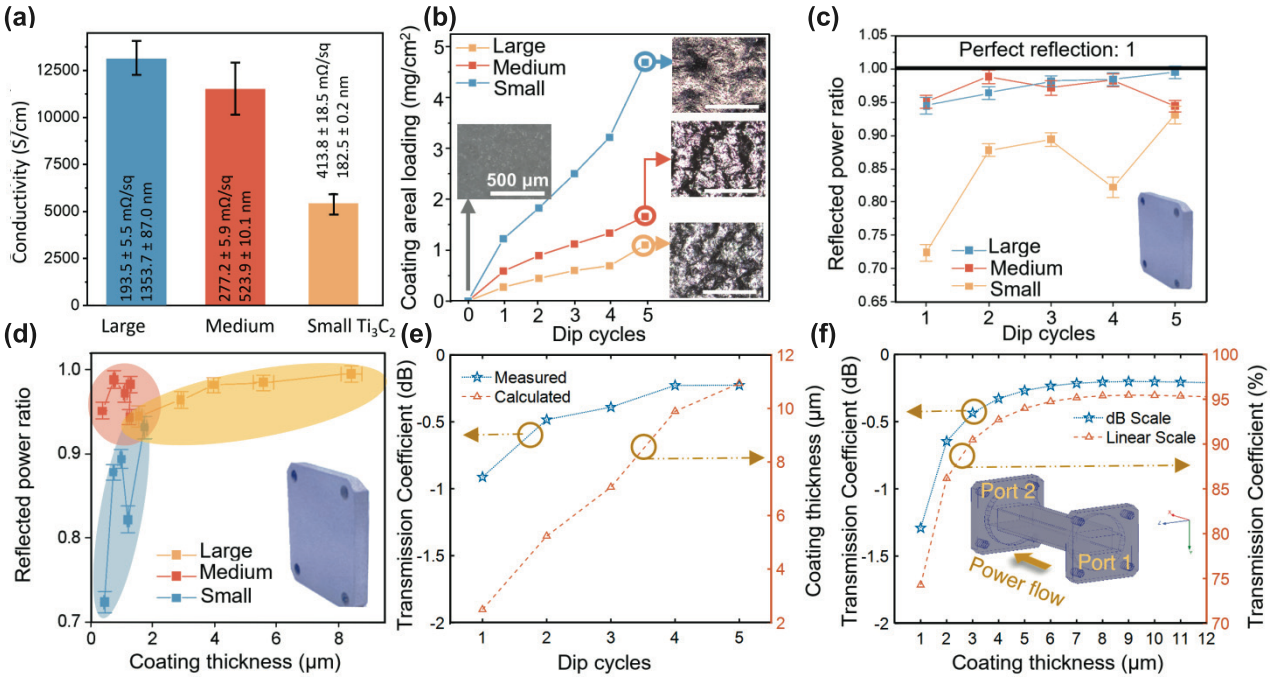

FIG. 2

Parametric performance optimization using MXene dispersions of different flake sizes and consecutive dip coating cycles. (A) Electrical conductivity, sheet resistance and flake size distribution of MXene dispersions of 3 different flake sizes. (B) MXene loading (mg cm^{-2}) on 3D printed coupons with 1 to 5 dips in MXene dispersions of 3 different flake sizes. Insets include the optical microscopy pictures of a pristine coupon and the coated coupons after 5 dips in MXene dispersions of 3 different sizes. (C) Microwave reflected power of the dip-coated coupons (D). Microwave reflected power versus estimated MXene coated thickness of the coupons based on MXene loading, roughness-counted coating surface area and vacuum-assisted film density of 3500 kg m^{-3}. (E) Measured transmission coefficient after every coating cycle in a dispersion of medium-sized MXene flakes (~500 nm) and the calculated thickness of MXene for coated coupons at each cycle. (F) Simulated transmission coefficient (dB and linear scale) for coating thicknesses ranging from 1 μm to 12 μm (The transmission coefficients were averaged over the monitored spectra and inset shows the structure of the straight waveguide).

Microwave measurements of the coupons were performed using a WR-90 Keysight waveguide calibration kit (8.2–12.4 GHz). The system was calibrated for one-port measurements. Fig. 2C shows that large and medium-sized MXene coatings exhibited significantly higher reflected power compared to small-sized MXene. With just one dip coating cycle, large and medium-sized MXene resulted in reflected power greater than 0.95. Moreover, large-sized MXene flakes showed a steady increase in reflected power with dip coating cycles, while small and medium-sized MXene coated samples exhibited small fluctuations in reflected power over the dip coating cycles. The performance fluctuation was attributed to the higher surface roughness of medium and small-sized MXene coated coupons, leading to less stable contacts between flakes. The reflected power of the coupons was plotted against the surface-normalized coating thickness in Fig. 2D. It is to be noted that despite the higher MXene loading (mg/cm^2) from the medium-sized dispersion, the coating thickness was comparable to small due to the increased surface area. Nevertheless, medium-sized MXene offered better power, indicating the importance of MXene flake size and electrical conductivity on performance. To benchmark the performance, the reflected power of six vacuum-assisted films made from 0.5 ml and 1 ml of the three different MXene dispersions was measured (Fig. S10). All films exhibited nearly perfect reflection, outperforming the coatings at comparable thicknesses with the performance gap increasing with decreasing flake size. This suggests that the rough surface substrate disrupts the alignment and contacts between flakes, resulting in a realized electrical conductivity lower than that of films (vacuum assisted filtered films are used to approximate the optimal flake alignment and contacts of a given MXene flake size). For the purpose of this study, to use MXene coating (Fig. S11) as fast, cost-effective method to impart electrical conductivity to 3D printed parts, medium-sized MXene flakes is recommended as they provided sufficient reflection performance with a faster drying time (processing time) compared to large MXene flakes, while also providing a thin conformal coating with low MXene consumption. Subsequently, actual straight waveguides were dip coated in a 20 mg/ml MXene dispersion of medium size (~500 nm), and the transmission coefficient was measured.

The functionality and performance of the MXene-coated structures were parametrically investigated through experiments and finite element method (FEM) simulations, observing a relation between the number of dip coating cycles and measured microwave performance (transmission coefficient) (Fig. 2E). This was then hypothetically tied to the thickness of the MXene coating and the effective electrical conductivity of a layer. The results depicted in Fig. 2E indicate the increasing number of dip-coating cycles resulted in a mass increase of the coated coupon. The observed mass change was perceived as a build-up of the MXene with increasing layer thickness. Furthermore, it was observed that, with increasing the number of dip coating cycles from one to four, the average transmission coefficient over the monitored frequency range improved by 14 % (+0.7 dB), with the highest measured efficiency of 95 % (-0.2 dB). Simulating MXene-based waveguides (using a FEM method) provided

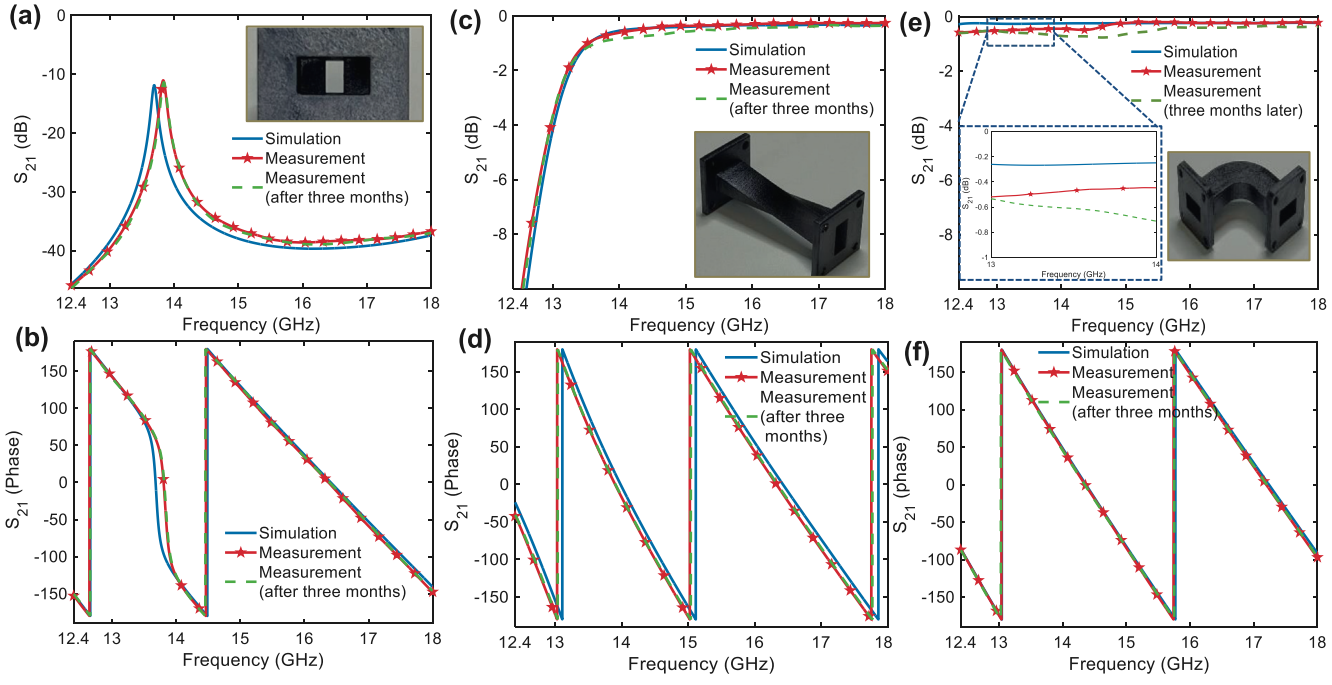

FIG. 3

Measurements and simulations of various implemented geometries, including the repeated measurements after three months of fabrication. The plots represent the magnitude and phase of the transmission coefficient in the measured spectra. (A), and (B): Resonating (filter) section. (C) and (D) twisted, polarization rotating section, (E) and (F) bent (90°) section.

additional support to performance enhancement by increasing thickness or electrical conductivity in the layer (Fig. 2F, Fig. 2E, Fig. S12 and the supplementary text).

To demonstrate the wide applicability of the proposed method for manipulating electromagnetic wave behavior, four different MXene-coated structures with complex geometries were manufactured and studied in the microwave regime (Fig. 3). These geometries are difficult for metal AM. Our measurement results demonstrated the suitability of the proposed method for producing a variety of MXene-based components with varying geometries (Fig. S13 – Fig. S15) and operation conditions (**Fig. S17-18** and supplementary text) after one dip coating cycle. To show the feasibility of a relatively complex geometry, a two-dimensional twist was 3D-printed, MXene-coated, and its transmission response was measured (Fig. 3C and 3D). The twisted sections are generally utilized to rotate the wave polarization in microwave signals (Fig. S15), physical equivalence of orientating waveguide apertures. In an optimized scenario, the twist should be gradually applied over a distance of two times the wavelength (the lowest operating frequency in this case, i.e., 12.4 GHz). Passing the stall frequency, the twist functioned as an effective guiding medium, with a low insertion loss of −0.27 dB, corresponding to a 6 % loss (relative to the input power) of transmitted electromagnetic power. The microwave oscillation phenomenon (Fig. 3A and 3B) and bent waveguiding (Fig. 3E and 3F) were also experimentally investigated with MXene-coated polymeric waveguides and the longevity of coating on these structures was investigated over three months and assessed as excellent (Fig. 3).

The power handling capability of MXene guides was studied by adjusting the input power of the signal source from + 20 dBm to + 40 dBm, covering the typical power levels utilized in LEO satellite communications [7]. At each input power level, measurements were taken after one hour of signal propagation through the waveguide. Fig. 4 shows the magnitude of the transmission coefficient for the varied power levels, and Fig. S16 includes the reflection coefficients and phase measurements for the transmission coefficient. The waveguides efficiently handled an input power level of 30 dBm (equivalent to 1 W) and 40 dBm (equivalent to 10 W), with no decline in performance. The frequency dependence of the transmission coefficient (Fig. 4, zoomed-in) shows that the transmission of electromagnetic power remains nearly identical across various input power levels, with a maximum change of 0.002 dB, equivalent to a relative difference in power transmission of 0.05 %. The insignificant variation observed across input power levels can be attributed to the minimal resolution of the microwave instrumentation utilized for detecting these power levels at the second port of the waveguide.

Finally, MXene-based waveguides for operation in different frequency bands, including LEO frequencies, were manufactured and measured. Fig. 5A demonstrates three MXene-coated waveguides for operation at different frequencies: X-band (WR-90 8.2–12.4 GHz range), Ku-band (WR-62 in 12-18 GHz range), and the K/Ka-band (WR-34 in 22–33 GHz range), which were manufactured using the proposed method (dimensions in Fig. S13). The X-band waveguide (Fig. 5B) demonstrated a −0.06 dB reduction in the transmission, compared to a metallic waveguide. This was equivalent to ~ 2 % of additional losses as a result of replacing metal with MXene in the same geometry. The K/Ka-band waveguide demonstrated increased losses in the 22–33 GHz range. Fig. 5D shows the measured transmission coefficient for a waveguide with operation frequency covering K and Ka bands (WR-34 waveguide) (dimensions and performance in **Fig. S13**). The reduced guiding performance of K/Ka-band waveguides is attributable to higher frequencies having a higher loss of microwaves within conductor bodies (relation to Eq. (1) described in the Supplementary Information). This indicated that the MXene coating thickness and conductivity should be further optimized for use in the high-frequency K/Ka range. Furthermore, the observed differences between simulated and measured waveguide performances (~1%, ~2%, and ~ 6 %, for X, Ku, and K/Ka bands, respectively) are attributed to fabrication-related parameters, such as film conductivity, roughness, and film thickness,

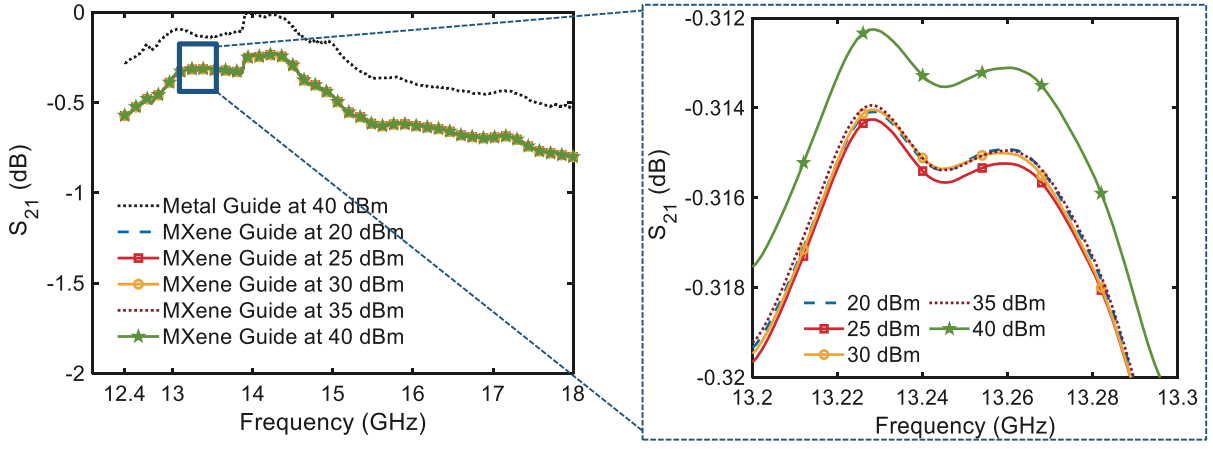

FIG. 4

Evaluation of MXene waveguides for high power (>20 dBm) handling capability. The power handling capability is demonstrated through the transmission coefficient of the MXene waveguides, at levels currently in use in LEO satellite systems.

and indicate the significance of parameter optimization for increasing the transmission coefficient of MXene-based waveguides.

The longevity of MXene-coated waveguiding components was verified through tests conducted six months after the coating, as shown in Fig. S20. The MXene-based waveguides were kept unsealed and stored under standard room conditions in a laboratory setting. The MXene guide had a slightly lower performance than its metallic counterpart, with a difference of −0.25 dB (equivalent to 6 % underperformance). For space applications, where components might experience extreme low temperatures, the electrical conductivity of Ti_3C_2 exhibits a slight increase down to at least ∼ 100 K (typical for metallic conductors) [43]. Therefore, excellent performance of the MXene-coated communication components is anticipated.

Over the past several decades, efforts have been made to reduce the weight in aerospace and satellite components by developing novel materials and manufacturing procedures and aiming for a certain level of operational efficiency. Moreover, with the recent expansion in satellite communications and extended space missions, the considerations for weight reduction has become crucial. Graphene, carbon nanotubes (CNTs), and conducting polymers (particularly, PEDOT: PSS) were also used as conducting materials in microwave technology in aerospace applications. However, only a limited number of structures based on graphene and CNTs have been reported for purposes other than absorption and EMI shielding, specifically for transmission and radiation applications [44–50]. A comparison of performance and manufacturability between MXene-based 3D waveguides and other nanomaterials in Table S1 shows that the MXene films offer higher shielding effectiveness and conductivity compared to films and coatings based on graphene, CNTs, and PEDOT: PSS [29]. Graphene and CNT-based materials may be used for microwave absorption and signal dissipation [46–50]. Furthermore, the reported non-reciprocal characteristics of graphene [51] may not be suitable for applications such as microwave guiding and transmission, which rely on reciprocity. Since solution-processable CNTs, reduced graphene oxide and polymer films don't offer sufficient conductivity and shielding effectiveness, and chemical vapor deposition of graphene onto polymers or transfer inside waveguide channels of a complex shape is not possible, we see MXene as the best available material for 3D waveguides.

Future work

In this study, we have demonstrated the effectiveness of MXene coatings applied to several waveguide geometries. The process is not limited to 3D printing and can be applied to polymeric waveguides Manufactured by other methods. It would be useful to compare performance of AM parts with conventionally processed parts, such as injection-molded or machined components, in follow-up studies. This comparison is crucial for commercialization, particularly in situations where faster and higher-volume production is essential. A systematic study of the impact of the type of MXene, MXene flake size and coating thickness on

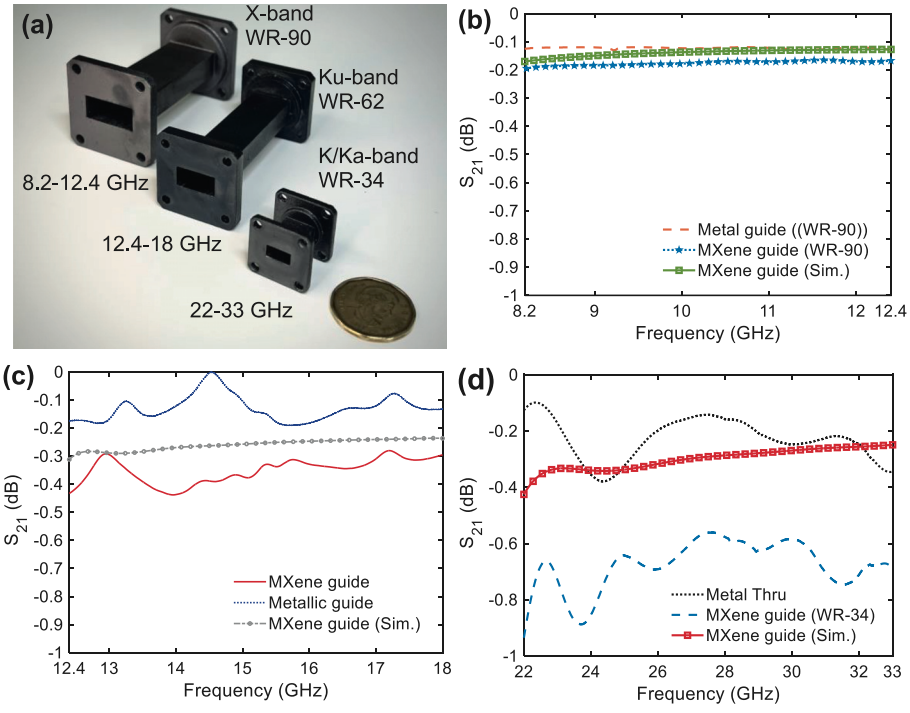

FIG. 5

Demonstration of MXene waveguides operating in different frequency bands, currently in use for (LEO) satellite communications. (A) Photograph of developed X-band, Ku-band, and K/Ka band waveguides, covering an operation range of 8 GHz to 33 GHz. (B) The measured transmission coefficient of X-band, MXene waveguide. (C) The measured transmission coefficient of Ku-band, MXene waveguide. (D) The measured transmission coefficient of K/Ka-band, MXene waveguide.

coating adhesion, following ASTM standards, and microwave reflectivity would certainly allow further improvements in performance.

Conclusions

This work showed that MXene coatings supported on additively-manufactured polymeric components can replace traditionally-manufactured channels of metallic waveguides. The benefits of the method include not only weight and cost of manufacturing, but also the feasibility of creating complex 3D-printed shapes that are much more difficult to make with metal. It can be expected that the manufacturability and processability of MXenes will allow for adjustment of microwave performance and manufacturing of a large variety of waveguides of any size and complexity beyond what was demonstrated in this work, also on the orbit. MXene coating can be accomplished by several methods and the choice of the substrate (the 3D-printed material) is not restricted to nylon but can include a variety of plastics, polymers, and composites. Also, the variety of MXenes allows the integration of thin films with different optical and structural properties for a multitude of industries, beyond waveguides and aerospace.

Materials and methods

To maintain the briefness of the main manuscript, a full description of materials, methods, and the details of this research work is provided in the Supplementary Information.

CRediT authorship contribution statement

Omid Niksan: Data curation, Investigation, Methodology, Writing – original draft, Writing – review & editing. **Lingyi Bi:** Data curation, Formal analysis, Methodology, Investigation, Writing – original draft, Writing – review & editing. **Kasra Khorsand Kazemi:** Methodology, Writing – review & editing. **Roman Rakhmanov:** Methodology, Writing – original draft, Writing – review & editing. **Yury Gogotsi:** Formal analysis, Funding acquisition, Methodology, Supervision, Validation, Writing – original draft, Writing – review & editing. **Mohammad H. Zarifi:** Conceptualization, Formal analysis, Funding acquisition, Investigation, Methodology, Project administration, Supervision, Validation, Writing – original draft, Writing – review & editing, Resources.

Data availability

Data will be made available on request.

Declaration of competing interest

The authors declare the following financial interests/personal relationships which may be considered as potential competing interests: Authors declare that they have no competing interests. A provisional patent has been filed in the U.S. Patent and Trademark Office (USPTO).

Acknowledgment

Funding and resources: Development of MXenes at Drexel University was supported by the National Science Foundation, United States (grant DMR-2034114). The UBC authors respectfully acknowledge the Syilx Okanagan Nation for the use of their unceded territory, the land on which this research was conducted. We acknowledge the support from Rogers Corporation for substrate donations and CMC Microsystems for providing software licenses. The authors acknowledge the financial support from the Department of National Defense of Canada (Contract No: W7714-196962/008/A) and the support from the Natural Sciences and Engineering Research Council of Canada (NSERC), through grant RGPIN-2018-04288 and the Canadian Foundation for Innovation (CFI) through grant no. 38148 and 37904. The UBC authors thank Aaryaman Shah, for his efforts in the prototyping and 3D printing.

Author contributions: Omid Niksan performed the design, fabrication, experimental/numerical investigations of the implemented waveguiding components. Lingyi Bi conducted MXene synthesis and characterization of MXene flakes and coatings. Kasra Khorsand Kazemi conducted the literature review. Roman Rakhmanov conducted a parametric performance study. Yury Gogotsi supervised MXene development, testing and characterization. Mohammad H. Zarifi conceptualized and designed the study, supervised the microwave analysis, as well as the performance investigations, supervised the research team and secured funding for the project. All authors contributed to writing and editing of the manuscript.

Appendix A. Supplementary data

Supplementary data to this article can be found online at https://doi.org/10.1016/j.mattod.2023.12.013.

References

[1] J.B. Roca et al., Nat. Mater. 15 (2016) 815–818.
[2] D. Gu et al., Science 372 (2021) eabg1487.
[3] M. Shusteff et al., Sci. Adv. 3 (2017) eaao5496.
[4] M. Han, Y. Liu, R. Rakhmanov, C. Israel, M.A.S. Tajin, G. Friedman, V. Volman, A. Hoorfar, K.R. Dandekar, Y. Gogotsi 2003225-1–7, Adv. Mater. 33 (2021).
[5] D.M. Pozar, fourth ed., Wiley, 2012.
[6] Z. Xiao et al., IEEE Wirel. Commun. (2022) 1–8.
[7] G. Amendola et al., IEEE Microw. Mag. 24 (2023) 32–48.
[8] I. Arregui et al., IEEE Microw. Mag. 21 (2020) 46–57.
[9] V.E. Boria, B. Gimeno, IEEE Microw. Mag. 8 (2007) 60–70.
[10] O. Niksan, J.D. Fowler, V. Balasubramanian, A. Shah, S. Pakpour, M.H. Zarifi, A waveguide resonator sensor for bacterial growth monitoring: towards antibiotic susceptibility testing, in: 2023 IEEE/MTT-S Int. Microw. Symp. - IMS 2023, IEEE, San Diego, CA, USA, 2023. https://doi.org/10.1109/IMS37964.2023.10188101.
[11] O. Niksan, A. Shah, M.H. Zarifi, Waveguide iris sensor with thermal modulation for non-intrusive flow rate measurements, in: 2022 IEEE MTT-S Int. Microw. Symp., IEEE, Denver, CO, USA, 2022. https://doi.org/10.1109/IMS37962.2022.9865459.
[12] C. Tomassoni et al., IEEE Microw. Mag. 21 (2020) 24–45.
[13] M. Li, Y. Yang, IEEE Microw. Mag. 24 (2023) 30–45.
[14] O. Niksan, M.C. Jain, A. Shah, M.H. Zarifi, IEEE Trans. Microw. Theory Tech. (2022) 1954–1963.
[15] O. Niksan, K. Colegrave, M.H. Zarifi, IEEE Trans. Microw. Theory Tech. 71 (2023) 698–709.
[16] Z. Azimi Dijvejin et al., Nat. Commun. 13 (2022) 5119.
[17] N.R. Tanguy et al., Chem. Eng. J. 466 (2023) 143061.
[18] K. Golvin, M. Zarifi, B. Wiltshire, K. Mirshahidi, R. Kozak, Method and apparatus for detecting ice formation on a surface using resonant sensors, 2020. https://patents.google.com/patent/US20220244195A1/en.
[19] M. Daneshmand, M.H. Zarifi, Apparatus and method for high resolution complex permittivity sensing using high-Q microwave sensors for lossy or non-lossy mediums and samples, 2018. https://patents.google.com/patent/US10175179B2/en.
[20] R. Melentiev et al., Mater. Des. 221 (2022) 110958.
[21] M. Boholm, R. Arvidsson, J. Clean. Prod. 68 (2014) 135–143.

[22] A. Kamyshny, S. Magdassi, Small 10 (2014) 3515–3535.
[23] B. Anasori, Y. Gogotsi, Springer, 2019.
[24] A. VahidMohammadi, J. Rosen, Y. Gogotsi, Science 372 (2021) eabf1581.
[25] V. Orts Mercadillo et al., Adv. Funct. Mater. 32 (2022) 2204772.
[26] T.S. Mathis et al., ACS Nano. 15 (2021) 6420–6429.
[27] M. Naguib, M.W. Barsoum, Y. Gogotsi, Adv. Mater. 33 (2021) 2103393.
[28] A. Iqbal et al., Science. 369 (2020) 446–450.
[29] F. Shahzad et al., Science. 353 (2016) 1137–1140.
[30] A. Sarycheva et al., Sci. Adv. 4 (2018) eaau0920.
[31] Y. Shao et al., Nat. Commun. 13 (2022) 3223.
[32] O. Niksan et al., Small. (2023) 2300848.
[33] K.K. Kazemi et al., Adv. Mater. Interfaces. 9 (2022) 2102411.
[34] S. Abdolhosseinzadeh et al., Mater. Today. 48 (2021) 214–240.
[35] C.E. Shuck et al., Adv. Eng. Mater. 22 (2020) 1901241.
[36] A. Levitt et al., Mater. Today. 34 (2020) 17–29.
[37] Y. Zhang et al., Nano Res. 15 (2022) 4916–4924.
[38] E. Li et al., ACS Appl. Mater. Interfaces. 13 (2021) 28996–29007.
[39] J. Liu et al., Adv. Electron. Mater. 6 (2020).
[40] L.X. Liu et al., Adv. Funct. Mater. 29 (2019).
[41] W. Hayt, J. Buck, McGraw Hill Education, 2019.
[42] R.P. Feynman, R.B. Leighton, M. Sands The new millennium ed., Basic Books, 2011.
[43] K. Hantanasirisakul, Y. Gogotsi, Adv. Mater. 30 (2018).
[44] M. Dragoman et al., Appl. Phys. Lett. 99 (3) (2011) 033112.
[45] T.G. Kang et al., Meas. J. Int. Meas. Confed. 137 (2019) 272–277.
[46] A. Saib et al., IEEE Trans. Microw. Theory Tech. 54 (2006) 2745–2753.
[47] S.K. Srivastava, K. Manna, J. Mater. Chem. A. 10 (2022) 7431–7496.
[48] X.X. Wang et al., Adv. Mater. 32 (2020) 2002112.
[49] G.C. Ghivela, J. Sengupta, IEEE Microw. Mag. 21 (2020) 48–65.
[50] J.G. Park et al., Nanotechnology. 20 (2009) 415702.
[51] D.L. Sounas, C. Caloz, IEEE Trans. Microw. Theory Tech. 60 (2012) 901–914.